ACS Chemical Neuroscience

Article

Synthesis and preliminary PET imaging studies of a FAAH radiotracer ([C]MPPO) based on #-ketoheterocyclic scaffold

Lu Wang, Joji Yui, Qifan Wang, Yiding Zhang, Wakana Mori, Yoko Shimoda, Masayuki Fujinaga, Katsushi Kumata, Tomoteru i Yamasak, Akiko Hatori, Benjamin H Rotstein, Thomas Lee Collier, Chongzhao Ran, Neil Vasdev, Ming-Rong Zhang, and Steven H Liang

ACS Chem. Neurosci., **Just Accepted Manuscript** • DOI: 10.1021/acschemneuro.5b00248 • Publication Date (Web): 27 Oct 2015

Just Accepted

ACS Publications

ACS Chemical Neuroscience is published by the American Chemical Society. 1155 Sixteenth Street N.W., Washington, DC 20036

Synthesis and preliminary PET imaging studies of a FAAH radiotracer ([^{11}C]MPPO) based on α-ketoheterocyclic scaffold

Lu Wang,[†,§] Joji Yui,[‡,§] Qifan Wang,[†] Yiding Zhang,[‡] Wakana Mori,[‡] Yoko Shimoda,[‡] Masayuki Fujinaga,[‡] Katsushi Kumata,[‡] Tomoteru Yamasaki,[‡] Akiko Hatori,[‡] Benjamin H. Rotstein,[†] Thomas Lee Collier,[†,¶] Chongzhao Ran,[#] Neil Vasdev,[†] Ming-Rong Zhang[*,‡] and Steven H. Liang[*,†]

[†] Division of Nuclear Medicine and Molecular Imaging, Massachusetts General Hospital & Department of Radiology, Harvard Medical School, Boston, MA, 02114, United States

[‡] Molecular Imaging Center, National Institute of Radiological Sciences, Chiba, 263-8555, Japan

[¶] Advion BioSystems, 10 Brown Road, Suite 101, Ithaca, New York, USA.

[#] Athinoula A. Martinos Center for Biomedical Imaging, Massachusetts General Hospital & Department of Radiology, Harvard Medical School, Charlestown, MA, 02129, United States

[§] These authors contribute equally to this work.

Supporting Information

ABSTRACT: Fatty acid amide hydrolase (FAAH) is one of the principle enzymes for metabolizing endogenous cannabinoid neurotransmitters such as anandamide, and thus regulates endocannabinoid (eCB) signaling. Selective pharmacological blockade of FAAH has emerged as a potential therapy to discern the endogenous functions of anandamide-mediated eCB pathways in anxiety, pain and addiction. Quantification of FAAH in the living brain by positron emission tomography (PET) would help our understanding of the endocannabinoid system in these conditions. While most FAAH radiotracers operate by an irreversible ('suicide') binding mechanism, a FAAH tracer with reversibility would facilitate quantitative analysis. We have identified and radiolabeled a reversible FAAH inhibitor, 7-(2-[^{11}C]methoxyphenyl)-1-(5-(pyridin-2-yl)oxazol-2-yl)heptan-1-one ([^{11}C]MPPO) in 13% radiochemical yield (non-decay corrected) with >99% radiochemical purity and 2 Ci/μmol (74 GBq/μmol) specific activity. The tracer showed moderate brain uptake (0.8 SUV) with heterogeneous brain distribution. However, blocking studies with a potent FAAH inhibitor URB597 demonstrated a low to modest specificity to the target. Measurement of lipophilicity, metabolite and efflux pathway analysis were also performed to study the pharmacokinetic profile of [^{11}C]MPPO. In all, we reported an efficient radiolabeling and preliminary evaluation of the first-in-class FAAH inhibitor [^{11}C]MPPO with α-ketoheterocyclic scaffold.

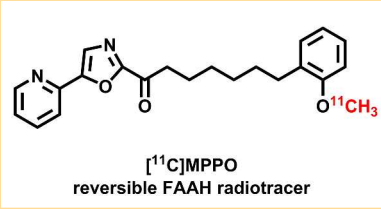

KEYWORDS: *PET, fatty acid amide hydrolase, FAAH, [^{11}C]MPPO, radiotracer*

INTRODUCTION

Endocannabinoid signaling systems is a neuromodulatory network which regulates mammalian neurophysiology, including cognition and memory, motor function, anxiety, pain perception, addiction and reward behaviors.[1] Endocannabinoids are endogenous small molecules (chemical messengers), and owing to their hydrophobic character which preclude storage into synaptic vesicles, they are biosynthesized and released 'on request' in vivo. The signaling network is modulated mainly via two G-protein-coupled receptors, namely, cannabinoid receptors CB1 and CB2. The corresponding endocannabinoid ligands of CB1/2 in mammals have been identified as anandamide (AEA)[2] and 2-arachidonoylglycerol (2-AG).[3,4] Early efforts have been focused on the direct pharmacological intervention of endocannabinoid system by its natural agonist

Δ⁹-tetrahydrocannabinol (the psychoactive component of Cannabis sativa) and other synthetic cannabinoids; however, the concomitant detrimental effects on cognition and motor control limit their use as therapeutic agents. In order to circumvent this problem, targeting enzyme degradation that controls endocannabinoid (AEA and 2-AG) levels has emerged as a potential strategy to identify drug candidates for medicinal uses.[5-9] Two enzymes, fatty acid amide hydrolase (FAAH) and monoacylglycerol lipase (MAGL) are primarily responsible for the degradation of AEA and 2-AG, respectively. In particular, FAAH is a ~60 kDa integral membrane enzyme that is highly expressed

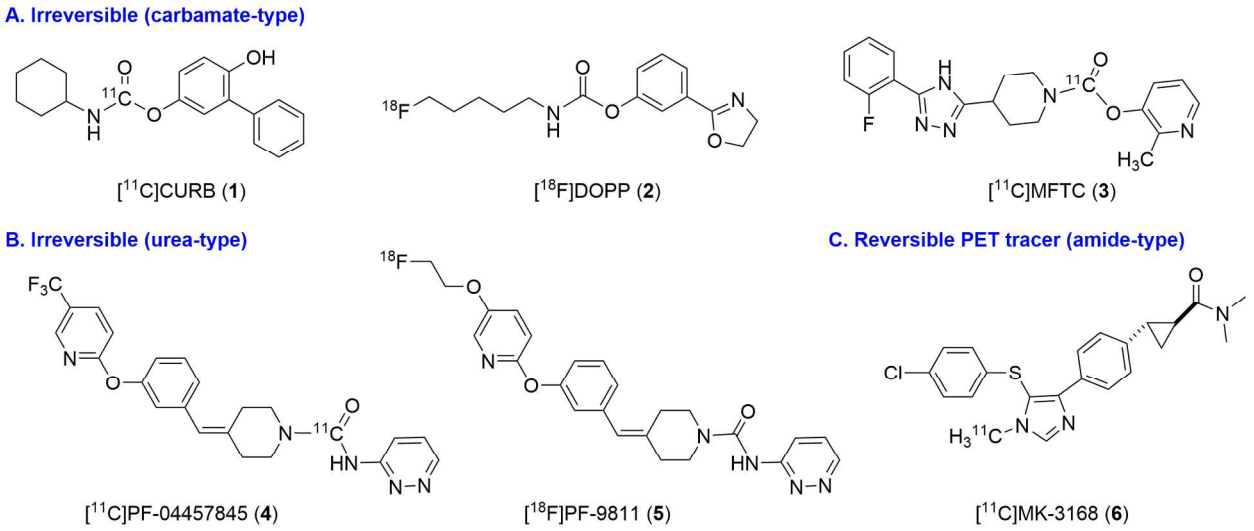

Figure 1. Representative PET radiotracers for imaging FAAH.

Scheme 1. Mechanism of action and this work.

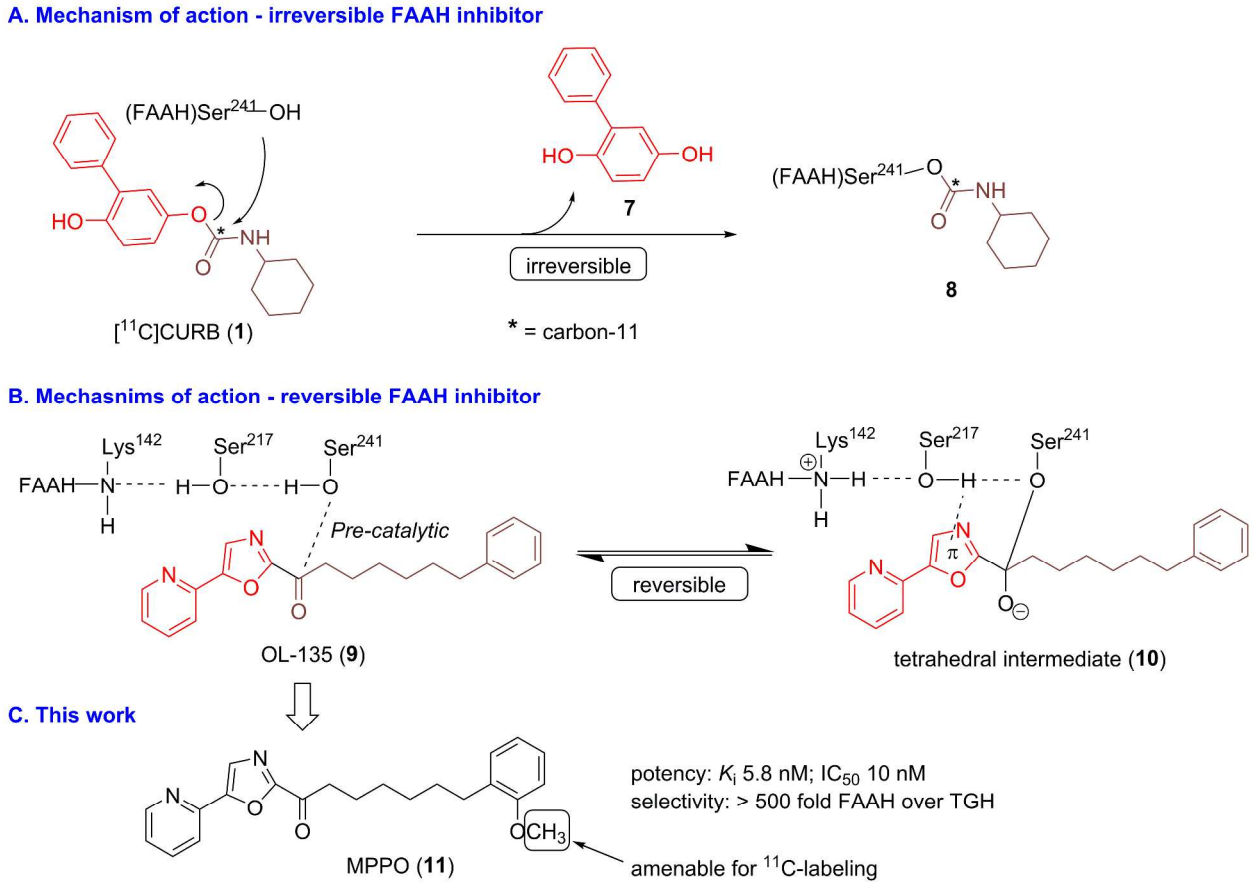

in the mammalian brain along with liver and kidney,[10,11] and functions as a serine hydrolase equipped with an unusual serine-serine-lysine (Ser241-Ser217-Lys142) catalytic triad.[12] Inhibition of FAAH increases the levels of AEA and has been found to reduce anxiety, pain, addiction and inflammation, as well as show anti-depressant and analgesic effects in preclinical models[13-15] without adverse effects in motility and behavior change observed with direct CB1 interventions.[16,17] Several reversible and irreversible FAAH inhibitors including URB597[16] and PF-04457845,[18-21] JNJ-42165279[22] and V158866[23] have advanced to clinical trials for release of osteoarthritis pain, cannabis withdrawal, anxiety and schizophrenia.

A positron emission tomography (PET) tracer for FAAH is desirable to allow quantitative enzyme mapping, target engagement and dose selection in clinical studies with high sensitivity under minimal perturbation of the biological state. As shown in Figure 1, there are continued efforts in the search for suitable FAAH PET tracers, including anadamide analogs,[24] [^{11}C-methyl]URB597 analog,[25] [^{11}C-carbonyl]URB694 ([^{11}C]CURB; **1**),[26,27] [^{18}F]DOPP (**2**),[28,29] [^{11}C]PF-04457845 (**4**),[30,31] [^{18}F]PF-9811 (**5**),[32] MK-3168 (**6**),[30] and most recently [^{11}C]MFTC (**3**).[33] To date, only two PET ligands have been reported in human studies, namely [^{11}C]CURB (**1**)[34,35] and [^{11}C]MK-3168 (**6**).[36] Although considerable advances have been made in the development of FAAH tracers, the majority of the reported radioligands are limited to suicide[37] inhibitors (Figure 1A-B), which feature a covalent irreversible binding mechanism. For instance, [^{11}C]CURB (**1**; Scheme 1A) binds to FAAH in vivo by acylation of the Ser241 sidechain and concomitant exclusion of unlabeled *O*-phenoxy fragment (**7**) to yield ^{11}C-labeled FAAH (**8**). As the first radiotracer for FAAH in humans, [^{11}C]CURB has been successfully utilized to map FAAH in the living brain using an irreversible two tissue compartment model.[34] However, based on the binding mechanism, [^{11}C]CURB only provides the measurement of FAAH activity, as opposed to FAAH availability,[29] which could be extracted from a reversible tracer as used in a ligand-receptor scenario in PET studies.[38] A FAAH tracer with reversibility would allow us to access key information from PET quantifications, including volumes of distribution, binding potentials, and monitor neurological response to therapeutics (occupancy and displacement studies).[39,40] To date, [^{11}C]MK-3168 (Figure 1C) is the only reversible PET ligand for this target and has advanced to human PET studies,[31] but only preliminary proceedings have been reported since 2012.[22,36] Therefore there is an urgent need for reversible FAAH radiotracers to address these questions and provide a full quantitative assessment of FAAH distribution, concentration, and activities in brain, to establish it as a viable biomarker for the diagnosis and prognosis of patients with associated disorders in endocannabinoid signaling system.

With the goal to develop a novel and reversible FAAH radiotracer, we aimed to design a ^{11}C-labeled molecule based on a potent and selective FAAH inhibitor, 7-phenyl-1-(5-(pyridin-2-yl)oxazol-2-yl)heptan-1-one (OL-135; **9**) with an established reversible binding mechanism (Scheme 1B).[41,42] Briefly, the hydroxyl group in Ser241 residue of FAAH is added to the carbonyl moiety of OL-135 to form an enzyme-bound intermediate (**10**), which is further stabilized by hydrogen bonding between FAAH(Ser217) and the oxazole ring. The tetrahedral intermediate **10** is covalently bound to FAAH(Ser241), but in a reversible manner, because the reaction cannot proceed further to release a leaving group. On the basis of these findings, we speculated that a positron-emitting analog of OL-135 would provide a potential reversible PET ligand for FAAH based on the existing mechanism of action. Therefore, we selected a recently reported close analog of OL-135, 7-(2-methoxyphenyl)-1-(5-(pyridin-2-yl)oxazol-2-yl)heptan-1-one (MPPO; **11**, Scheme 1C), which is amenable for ^{11}C-labeling and exhibited an excellent binding profile[43] to FAAH in vitro with IC_{50} value of 10 nM and greater than 500 fold selectivity over triacylglycerol hydrolase (TGH) as well as > 10^5 fold selectivity over hydrolytic enzyme KIAA1363. Herein we describe our synthesis, radiolabeling and preliminary evaluation of [^{11}C]MPPO, the first-in-kind α-ketoheterocyclic PET ligand targeting FAAH.

RESULTS AND DISCUSSION

Chemistry. With MPPO **11** as the target, we designed a synthetic strategy for the synthesis (for detailed retrosynthetic analysis, see Scheme S1 in Supporting Information). As summarized in Scheme 2A, 5-(pyridin-2-yl)oxazole (**14**) was constructed in a quantitative yield according to the literature procedure.[43-45] Protection of alcohol **15** with 3,4-dihydro-2*H*-pyran in the presence of a catalytic amount of PPTS afforded bromide **16** in 85% yield. Condensation of 2-methoxybenzaldehyde with Wittig salt **17** afforded the mixture of *Z*/*E* olefins **18** in a yield of 56% over two steps. It was worthy of note that the synthesis of Wittig salt **17** in organic solvents, such as THF, toluene or CH3CN, led to low to modest yields of **18** (0-21%). The optimized reaction parameters were identified as solvent-free conditions in neat PPh3 at 120 °C for 4 h to generate **17**, which was utilized in the subsequent Wittig olefination immediately. Compound **19** was obtained in 99% yield on exposure to a Pd/C catalyzed hydrogenation of **18** and the subsequent deprotection with TsOH yielded **20**. Swern oxidation afforded aldehyde **21** in 83% yield. The synthesis of key intermediate **22** was not straightforward since base-mediated condensation using KHMDS, LHMDS, *n*BuLi, *n*BuLi/Bu_3SnCl, *n*BuLi/$ZnCl_2$/CuI or MeMgBr failed to produce the desired product. A notable improvement was achieved when *i*PrMgCl in THF was used, leading to the secondary alcohol **22** in almost quantitative conversion. Compound **22** was used without further purification in the following Dess-Martin oxidation to generate MPPO (**11**) in 51% yield. Demethylation of **11** with BBr_3 in CH_2Cl_2 gave the radiolabeling precursor phenol (7-(2-hydroxyphenyl)-1-(5-(pyridin-2-yl)oxazol-2-yl)heptan-1-one; **23**) in 58% yield after recrystallization.

Scheme 2. Syntheses of standard and precursor, and radiolabeling of [^{11}C]MPPO

A. Synthetic Route for MPPO

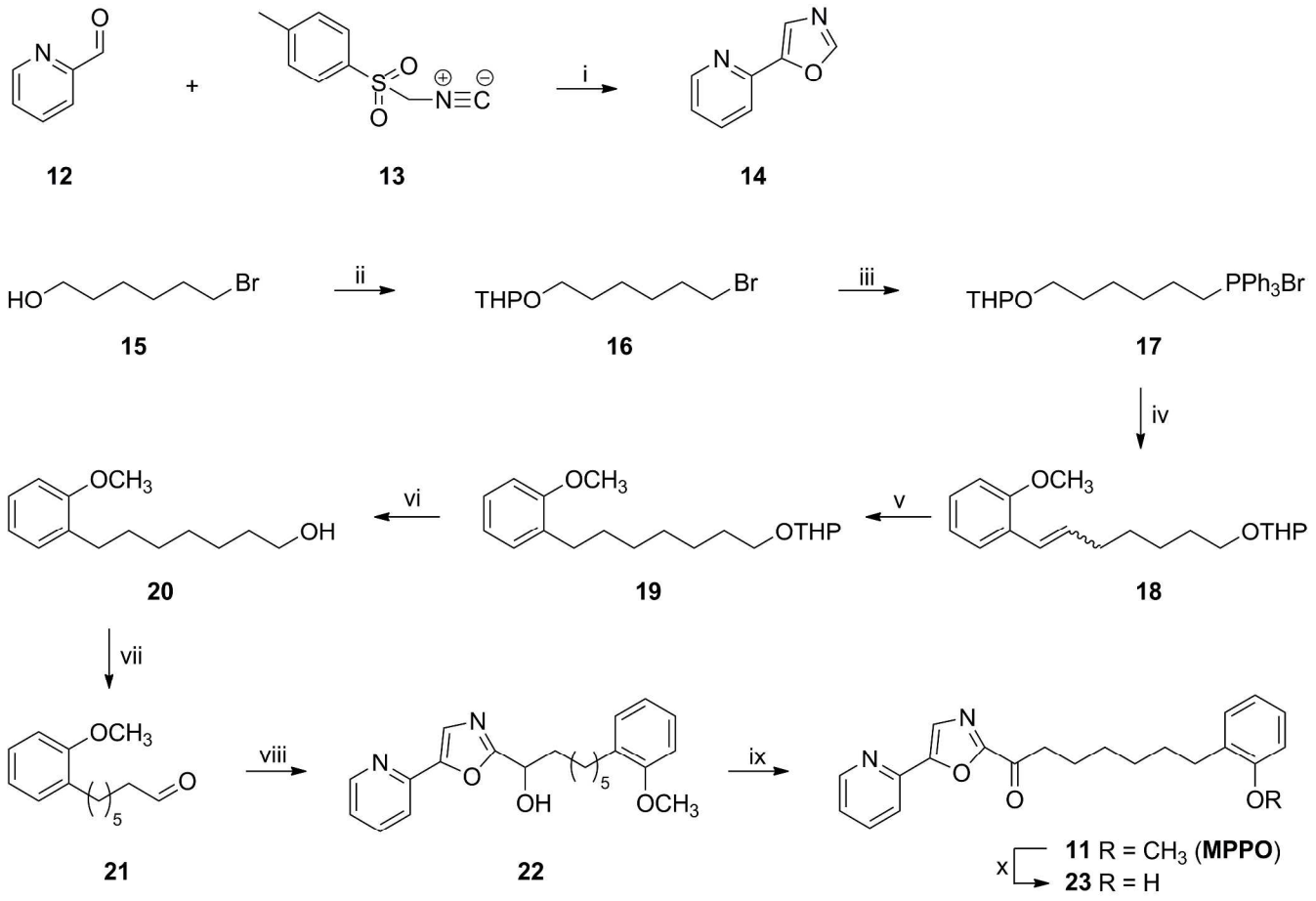

B. Radiolabeling of [^{11}C]MPPO

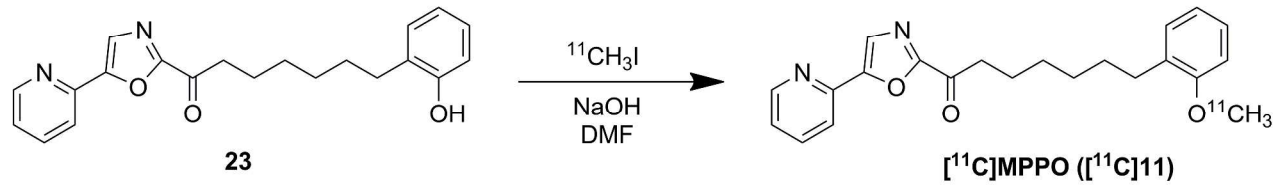

[a]Reagents and conditions: (i) K_2CO_3, MeOH, 96%. (ii) 3,4-dihydro-2*H*-pyran, PPTS, CH_2Cl_2, 85%. (iii) PPh_3, 120 °C. (iv) 2-methoxybenzaldehyde, LiHMDS, THF, 56% over two steps. (v) Pd/C, H_2, MeOH, 99%. (vi) *p*-Toluenesulfonic acid monohydrate, MeOH, 89%. (vii) $(COCl)_2$, DMSO, Et_3N, CH_2Cl_2, 83%. (viii) **14**, *i*PrMgCl, THF. (ix) Dess-Martin periodinane, CH_2Cl_2, 51% over two steps. (x) BBr_3, CH_2Cl_2, 58%.

Radiolabeling. As shown in Scheme 2B, the methyl ether was identified as the most convenient labeling site for MPPO with carbon-11. The automated radiosynthesis of [^{11}C]MPPO was performed by the reaction of a phenolic precursor **23** with [^{11}C]CH_3I in the presence of NaOH. [^{11}C]CH_3I was bubbled through the reaction vial and after 5 min of reaction time at 80 °C, we observed highly selective conversion to [^{11}C]MPPO. The reaction mixture was purified by reverse phase HPLC, and reformulated in saline for intravenous injection. [^{11}C]MPPO was synthesized in 13 ± 3% radiochemical yields based on [^{11}C]CO_2 (non-decay corrected) for the subsequent preclinical PET imaging studies. Specifically, starting from 350 - 530 mCi (13.0 - 19.6 GBq) of [^{11}C]CO_2, [^{11}C]MPPO was obtained in 58 ± 17 mCi (2.15 ± 0.65 GBq) at end-of-synthesis (~29 min synthesis time from end-of-bombardment) with > 99%

radiochemical purity (n = 10; for semi-preparative and analytical HPLC results, see Figure S1 in Supporting Information). The specific activity was greater than 2 Ci/μmol (74 GBq/μmol) and no radiolysis was observed within 90 min after formulation.

In a parallel approach, we also prepared an aliphatic analog of OL-135 for radiolabeling. Swern oxidation of alcohol **24** gave the corresponding aldehyde **25** in 70% yield. After a sequential *i*PrMgCl-mediated condensation and Dess-Martin oxidation, radiolabeling precursor bromide **26** was obtained in a yield of 72% over two steps. The resulting bromide **26** was subjected to nucleophilic displacement with KF and 18-crown-6 in CH_3CN to give the corresponding fluoro analog **27** in 30% yield after recrystallization. The radiofluorination proceeded to generate [^{18}F]**27** in 3% isolated radiochemical yield with greater than 1 Ci/μmol specific activity; however, further evaluation was not pursued due to a rapid defluorination in vivo (Scheme S2 in Supporting Information).

Table 1. Distribution of radioactivity in mice after injection of [^{11}C]MPPO. Data are %ID/g (mean ± SD, n = 3)

tissue	1 min	5 min	15 min	30 min	60 min
blood	1.83 ± 0.15	0.75 ± 0.07	0.38 ± 0.03	0.34 ± 0.05	0.30 ± 0.01
heart	6.89 ± 0.60	1.65 ± 0.07	0.55 ± 0.01	0.51 ± 0.03	0.32 ± 0.03
lungs	17.47 ± 3.88	4.88 ± 0.41	1.20 ± 0.04	1.19 ± 0.18	0.64 ± 0.08
liver	9.78 ± 1.10	18.61 ± 2.31	20.05 ± 1.43	17.47 ± 1.10	13.69 ± 0.63
spleen	2.28 ± 0.50	1.29 ± 0.22	0.60 ± 0.03	0.49 ± 0.03	0.37 ± 0.01
kidneys	12.64 ± 0.56	17.17 ± 1.67	13.70 ± 0.69	9.55 ± 0.65	6.20 ± 0.70
small intestine	3.08 ± 0.29	7.22 ± 0.89	18.54 ± 4.00	15.72 ± 4.58	13.75 ± 3.44
testes	0.44 ± 0.05	0.67 ± 0.02	0.59 ± 0.00	0.48 ± 0.02	0.30 ± 0.03
muscle	1.78 ± 0.16	1.03 ± 0.09	0.58 ± 0.17	0.50 ± 0.17	0.24 ± 0.04
brain	1.87 ± 0.20	2.27 ± 0.16	1.81 ± 0.09	1.40 ± 0.15	0.88 ± 0.09

Lipophilicity. Lipophilicity of radiolabeled tracer has predictive utility for assessing blood-brain barrier permeability, with an optimum log*P* range of 2.0–3.5.[46-49]

Using liquid-liquid partition between *n*-octanol and PBS buffer (pH 7.4),[47] $logD_{7.4}$ of [^{11}C]MPPO was determined to be 3.43 (n = 3), which is comparable with several brain penetrant FAAH tracers, including [^{11}C]CURB (**1**; $logD_{7.4}$ 2.8),[26] [^{11}C]PF-04457845 (**4**; $logD_{7.4}$ 3.48).[30]

Whole body biodistribution studies in mice. The kinetics and tissue distribution of [^{11}C]MPPO was studied in mice at several experimental time points (1, 5, 15, 30 and 60 min) post-tracer injection. The results are expressed as the percentage of injected dose per wet tissue (%ID/g) in Table 1 (for biodistribution expressed as SUV unit, see Table S1 in Supporting Information). At 1 min post injection, a high uptake (> 3 %ID/g) was observed in the heart, lungs, liver, kidneys and small intestine. After the initial phase the radioactivity levels in most tissues decreased rapidly, while the signals in the liver and small intestine continually increased until 15 min and then decreased slowly. The radiotracer was efficiently cleared from blood (1 min/60 min ratio of 6.1) and high uptake of [^{11}C]MPPO in the liver, kidney, and small intestine suggests that hepatobiliary and urinary excretion, as well as the intestinal reuptake pathway, may dominate the whole body distribution of radioactivity. The present result indicates that the distribution of [^{11}C]MPPO was in agreement with the distribution of FAAH in mice as reported previously,[50-52] with high expression in the liver, brain, testes, kidneys and spleen. In addition, rapid clearance of radioactivity from lungs, heart and muscle was observed, which is consistent with low FAAH expression in these organs in mice.[50]

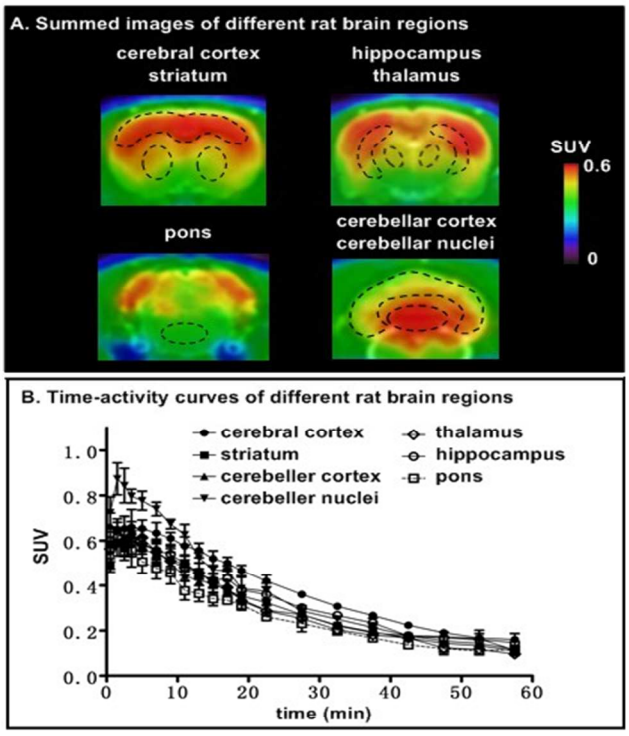

Figure 2. Representative coronal PET images (summed 0-30 min) and time-activity curves of [^{11}C]MPPO in different rat brain regions (n = 3, mean ± SEM).

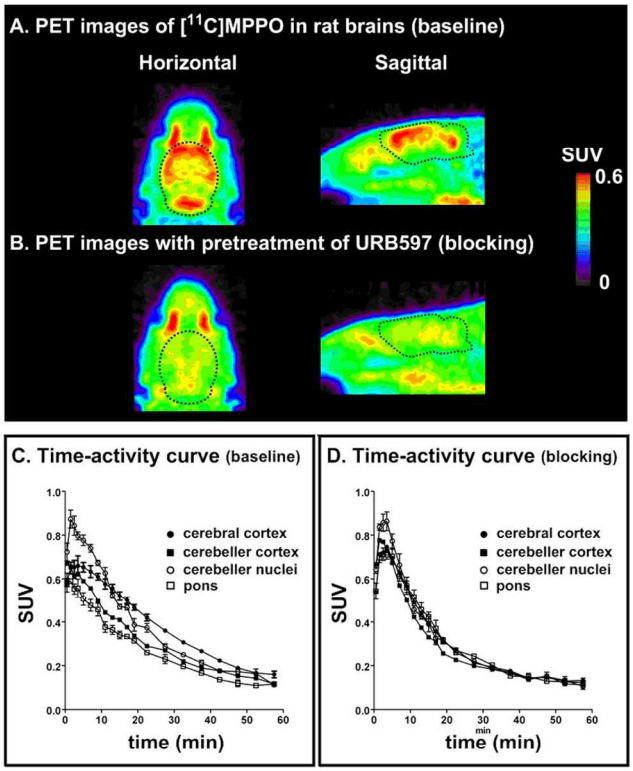

Figure 3. Representative PET images (0-30 min) and time-activity curves (baseline and blocking) of [^{11}C]MPPO in rat brains. (n = 3; mean ± SEM).

The total level of initial brain uptake of [^{11}C]MPPO was moderate to high with 1.87 %ID/g and 2.27 %ID/g at 1 min and 5 min post-tracer injection, respectively. The radioactivity washout from the brain was rapid with 0.88 %ID/g at 60 min time point (5 min/60 min ratio of 2.6). These results indicate moderate brain uptake (0.8 SUV) of [^{11}C]MPPO. Therefore we further evaluated [^{11}C]MPPO as a suitable reversible PET tracer for FAAH neuroimaging in PET imaging studies in Sprague-Dawley rats.

PET imaging studies in rats. Representative PET images of rat brain after injection of [^{11}C]MPPO are shown in Figure 2A. PET images in normal rats showed moderate brain penetration and accumulation of radioactivity in the brain. The highest radioactivity was seen in the cerebellar nuclei (0.87 SUV), followed by cerebral cortex, hippocampus, thalamus, striatum while the lowest uptake was observed in the pons. As shown in the time-activity curves of different brain regions, radioactivity in brain tissues increased rapidly after the injection of [^{11}C]MPPO, peaked at 1.5 min (0.87 SUV in cerebellar nuclei), and gradually washed out over 60 min. The distribution pattern of [^{11}C]MPPO was similar to that for [^{11}C]CURB[26] or [^{11}C]MFTC[33] and the distribution of FAAH in the rat brain.[51-54]

As shown in Figure 3, pretreatment with a potent FAAH inhibitor, URB597 (3 mg/kg, 30 min iv before injection), successfully abolished the difference of radioactivity uptakes in different regions of interest. The radioactivity distribution became fairly uniform in all brain regions,

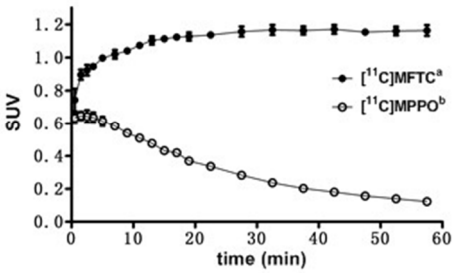

Figure 4. Reversible binding of [^{11}C]MPPO in the brain. (n = 3; mean ± SD). a. SUV data from PET imaging of [^{11}C]MFTC in rat whole brain; b. SUV data from PET imaging of [^{11}C]MPPO in rat whole brain.

including cerebral cortex, cerebellar cortex, cerebellar nuclei and pons, indicating certain specificity of [^{11}C]MPPO, albeit modest, to FAAH in the rat brains, although there was only a marginal difference of regional brain uptake between baseline and blocking.

[^{11}C]MPPO, as hypothesized in Scheme 1B, may show a reversible binding profile to FAAH (Figure 4). The radioactivity reached the maximum uptake of 0.65 SUV, follow by a steady washout in rat brains (5 min/60 min ratio of 5.1). Compared with an irreversible FAAH radiotracer [^{11}C]MFTC,[33] within 60 min post injection, no significant decrease of [^{11}C]MFTC in rat brain uptake was observed (5 min/60 min ratio of 0.9).

Metabolite analysis. To evaluate the in vivo stability of [^{11}C]MPPO, the fraction of radiometabolites in the plasma and brain homogenate of Sprague-Dawley rats was evaluated post-tracer injection. The percentages of unchanged [^{11}C]MPPO and the corresponding radiometabolites, as determined by radio-HPLC, are shown in Figure 5. Analysis of rat brain homogenates and plasma 15 min post-tracer injection showed that 75% and 90% metabolism occurred with the radioactivity associated with hydrophilic metabolites. These results indicates a rapid in vivo metabolism of [^{11}C]MPPO, which may contribute to the low specific binding and/or rapid washout in PET imaging studies.

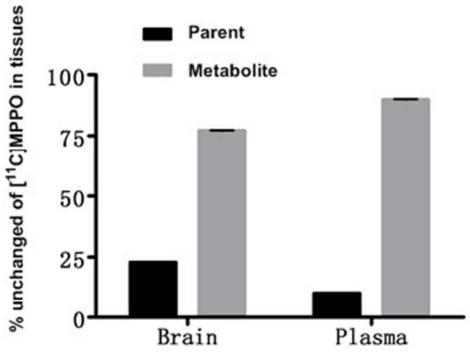

Figure 5. Radiometabolites of [^{11}C]MPPO in rats. (n = 3; mean ± SD)

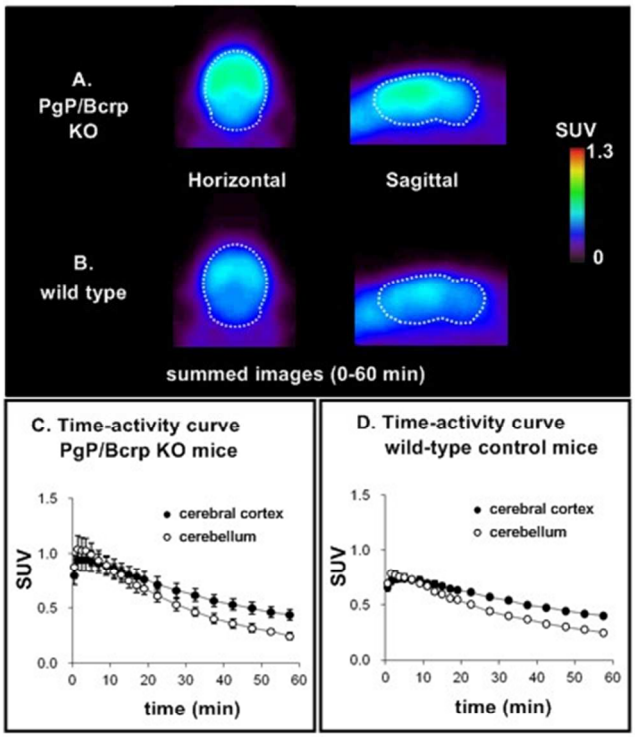

Figure 6. PET images (0-60 min) and time-activity curves in wild-type and PgP/BCRP KO mice (n = 3; mean ± SEM).

PET imaging studies in PgP/Bcrp knockout mice. Another possible reason for relatively a low-to-moderate brain uptake and/or specific binding of [^{11}C]MPPO in the brain could be insufficient brain penetration due to ATP-binding cassette (ABC) efflux transporters, including P-glycoprotein (PgP) and breast cancer resistance protein (Bcrp) at the blood-brain barrier.[40,55]

In order to evaluate the interaction between [^{11}C]MPPO and ABC transporters, we carried out PET imaging studies and compared radiotracer behavior, including brain uptake and washout on wild-type and PgP/Bcrp knockout mice (ABCB1a/1b$^{-/-}$ABCG2$^{-/-}$), in cerebral cortex and cerebellum regions. As shown in Figure 6, peak brain uptake in cerebral cortex and cerebellum was 0.95 SUV and 1.04 SUV in PgP/Bcrp KO mice, respectively, representing a marginal difference in comparison to the uptakes of cerebral cortex (0.74 SUV) and cerebellum (0.78 SUV) in wild type controls. In addition, brain uptakes in cerebral cortex and cerebellum of [^{11}C]MPPO was not noticeably increased in PgP/Bcrp KO mice compared with that of wild type mice (ratio of KO/WT in AUC[cerebral cortex]= 1.2 and ratio of KO/WT in AUC[cerebellum]= 1.2); therefore these results indicates [^{11}C]MPPO lacks intensive interactions with PgP/Bcrp efflux pump on the murine blood-brain barrier and is not likely a substrate for Pgp/Bcrp in mice.

CONCLUSION

We have efficiently synthesized a new α-ketoheterocyclic FAAH radioligand, [^{11}C]MPPO, in good radiochemical yield, high radiochemical purity and high specific activity. The lipophilicity, whole body distribution, brain penetration, efflux pump and metabolism studies were evaluated to determine the suitability of [^{11}C]MPPO as a FAAH radiotracer. Preliminary PET imaging studies showed low to moderate level of specific binding to FAAH in murine brains. Although [^{11}C]MPPO is less likely pursued for in vivo mapping of FAAH in the brain, the radiosynthesis and preliminary evaluation by PET imaging studies offers a roadmap for the investigation of other FAAH radiotracer candidates based on the α-ketoheterocyclic drug scaffolds with reversible binding profiles. In the future, radioligands with higher affinity and stability with minimal off-target binding will need to be developed to allow in vivo imaging of FAAH.

METHODS

Materials and Methods

Chemistry. *General Conditions*. All the chemicals employed in the syntheses were purchased from commercial vendors and used without further purification. Thin-layer chromatography (TLC) was conducted with 0.25 mm silica gel plates (60F-254) and visualized by exposure to UV light (254 nm) or stained with potassium permanganate. Flash column chromatography was performed using silica gel (particle size 0.040-0.063 mm). H-Nuclear magnetic resonance (NMR) spectra were obtained at 400 or 500 MHz on Bruker spectrometers in $CDCl_3$ solutions at room temperature with tetramethylsilane (TMS, δ = 0) as an internal standard. ^{13}C NMR spectra were obtained at 100 or 125 MHz and ^{19}F-NMR spectra were obtained at 376 MHz. Chemical shifts (δ) are reported in ppm and coupling constants are reported in Hertz. The multiplicities are abbreviated as follows: s = singlet, d = doublet, t = triplet, m = multiplet, br = broad signal, dd = doublet of doublets, etc. For all the HRMS measurements, the ionization method is ESI and the mass analyzer type is TOF.

*2-((7-(2-methoxyphenyl)hept-6-en-1-yl)oxy)tetrahydro-2H-pyran (**18**)*. Compound **16** (3.9 g, 14.7 mmol) and PPh_3 (5.8 g, 22.3 mmol) were placed in an oven-dried reaction vessel charged with a stir bar, which was filled with argon. The mixture was heated at 120 °C for 4 h, then cooled down to ambient temperature, followed by addition of THF (40 mL). The resulting mixture was stirred at room temperature for 10 min, then LiHMDS (1.0 M in THF, 18.4 mL, 18.4 mmol) was added slowly. The reaction was stirred for 1 h and cooled down to 0 °C. A solution of 2-methoxybenzaldehyde (1.8 g, 13.5 mmol) in THF (20 mL) was added into the reaction. The mixture was stirred overnight at room temperature, then diluted with EtOAc (70 mL), and washed with H_2O (30 mL x 1) and brine (30 mL x 1), dried over anhydrous Na_2SO_4, and concentrated. The residue was purified by flash chromatography on silica gel (hexanes to ethyl acetate gradient column) to yield the compound **18** as a yellow oil (2.3 g, 56% over two steps). R_f = 0.5 (Hexanes/EtOAc = 50/1); ^{1}H NMR showed the compound exists as a 1:0.6 mixture of *Z*- and *E*- products, which are used for the next step without further

separation; HRMS calcd for $C_{19}H_{29}O_3$ $(M + H)^+$ 305.2117, found 305.2121.

*7-(2-methoxyphenyl)-1-(5-(pyridin-2-yl)oxazol-2-yl)heptan-1-one (**11**).* To a solution of the compound **14** (219 mg, 1.5 mmol) in anhydrous THF (7 mL) at 0 °C was added *i*PrMgCl (2 M in THF, 0.9 mL, 1.8 mmol), the mixture was stirred at 0 °C for 1 h. A solution of compound **21** (330 mg, 1.5 mmol) in THF (4 mL) was added into the reaction, and the mixture was allowed to room temperature and stirred for 3 h and quenched with saturated aqueous NH_4Cl (10 mL) and extracted with EtOAc (3 x 10 mL). The organic layers were combined, washed with water (1 x 10 mL) and brine (1 x 10 mL), dried over Na_2SO_4, filtered and evaporated under reduced pressure. The residue was dissolved immediately into CH_2Cl_2 (10 mL). Dess-Martin periodinane (1.1 g, 2.6 mmol) was added to a solution and the resultant suspension was stirred at rt for 2 h. Then the reaction was quenched with saturated aqueous Na_2SO_3 solution (5 mL) and $NaHCO_3$ solution (5 mL), and the mixture was stirred for another 30 min. Then the aqueous layer was extracted with CH_2Cl_2 (3 x 7 mL). The combined organic portion was washed with brine (5 mL), dried over Na_2SO_4, filtered, and concentrated in vacuo. The residue was purified by flash chromatography on silica gel (hexanes to ethyl acetate gradient column) to yield the compound **11** as a white solid (278 mg, 51% over two steps). R_f = 0.7 (Hexanes/EtOAc = 2/1); ^{1}H NMR (400 MHz, $CDCl_3$) δ 8.68 (d, J = 4.8 Hz, 1H), 7.90-7.87 (m, 2H), 7.82 (td, J = 8.0, 1.6 Hz, 1H), 7.35-7.31 (m, 1H), 7.20-7.13 (m, 2H), 6.91-6.84 (m, 2H), 3.83 (s, 3H), 3.13 (t, J = 7.2 Hz, 2H), 2.62 (t, J = 7.6 Hz, 2H), 1.85-1.77 (m, 2H), 1.66-1.58 (m, 2H), 1.50-1.40 (m, 4H); ^{13}C NMR (100 MHz, $CDCl_3$) δ 188.5, 157.4, 153.2, 150.1, 146.3, 137.1, 131.0, 129.7, 126.8, 124.1, 120.3, 120.2, 110.1, 55.2, 39.1, 30.0, 29.6, 29.2, 29.0, 23.9; HRMS calcd for $C_{22}H_{25}N_2O_3$ $(M + H)^+$ 365.1865; found 365.1859.

*7-(2-hydroxyphenyl)-1-(5-(pyridin-2-yl)oxazol-2-yl)heptan-1-one (**23**).* To a solution of the compound **11** (428 mg, 1.17 mmol) in anhydrous CH_2Cl_2 (15 mL) at -78 °C was added BBr_3 (0.35 mL, 3.53 mmol), the mixture was allowed to room temperature and stirred for 1 h, and quenched with saturated aqueous $NaHCO_3$ (7 mL) and 10% NaOH (7 mL). The aqueous layer was extracted with CH_2Cl_2 (3 x 7 mL). The combined organic portion was washed with brine (10 mL), dried over Na_2SO_4, filtered, and concentrated in vacuo. The residue was purified by flash chromatography on silica gel (hexanes to ethyl acetate gradient column) to yield the crude product, which was recrystallized using 10% CH_2Cl_2/Hexanes to yield pure compound **23** as a white solid (238 mg, 58%). R_f = 0.4 (Hexanes/EtOAc = 2/1); ^{1}H NMR (500 MHz, $CDCl_3$) δ 8.68 (d, J = 4.8 Hz, 1H), 7.89-7.86 (m, 2H), 7.82 (td, J = 8.0, 1.6 Hz, 1H), 7.34-7.31 (m, 1H), 7.12-7.10 (m, 1H), 7.10-7.04 (m, 1H), 6.85 (t, J = 7.5 Hz, 1H), 6.76 (dd, J = 8.0, 0.5 Hz, 1H), 5.35-5.30 (m, 1H), 3.11 (t, J = 7.0 Hz, 2H), 2.62 (t, J = 7.5 Hz, 2H), 1.81-1.77 (m, 2H), 1.68-1.63 (m, 2H), 1.45-1.42 (m, 4H); ^{13}C NMR (125 MHz, $CDCl_3$) δ 188.5, 157.3, 153.5, 153.1, 150.0, 146.2, 137.1, 130.2, 128.5, 126.9, 126.8, 124.1, 120.6, 120.4, 115.1, 39.0, 29.7, 29.4, 28.9, 28.8, 23.8; HRMS calcd for $C_{21}H_{23}N_2O_3$ $(M + H)^+$ 351.1709; found 351.1702.

*12-bromo-1-(5-(pyridin-2-yl)oxazol-2-yl)dodecan-1-one (**26**).* To a solution of the compound **14** (500 mg, 3.42 mmol) in anhydrous THF (15 mL) at 0 °C was added *i*PrMgCl (2 M in THF, 2.1 mL, 4.2 mmol), the mixture was stirred at 0 °C for 1 h. A solution of aldehyde **25** (1.1 g, 4.2 mmol) in THF (10 mL) was added into the reaction, and the mixture was allowed to room temperature and stirred for 3 h and quenched with saturated aqueous NH_4Cl (7 mL) and extracted with EtOAc (3 x 10 mL). The organic layers were combined, washed with water (1 x 10 mL) and brine (1 x 10 mL), dried over Na_2SO_4, filtered and evaporated under reduced pressure. The residue was dissolved immediately into CH_2Cl_2 (30 mL). Dess-Martin periodinane (1.77 g, 4.18 mmol) was added to a solution and the resultant suspension was stirred at rt for 2 h. Then the reaction was quenched with saturated aqueous Na_2SO_3 solution (7 mL) and $NaHCO_3$ solution (7 mL), and the mixture was stirred for another 30 min. Then the aqueous layer was extracted with CH_2Cl_2 (3 x 15 mL). The combined organic portion was washed with brine (15 mL), dried over Na_2SO_4, filtered, and concentrated in vacuo. The residue was purified by flash chromatography on silica gel (hexanes to ethyl acetate gradient column) to yield the compound **26** as a white solid (997 mg, 72% over two steps). R_f = 0.25 (Hexanes/EtOAc = 10/1); ^{1}H NMR (400 MHz, $CDCl_3$) δ 8.67-8.65 (m, 1H), 7.87-7.85 (m, 2H), 7.80 (td, J = 7.6, 1.6 Hz, 1H), 7.32-7.29 (m, 1H), 3.39 (t, J = 6.8 Hz, 2H), 3.10 (t, J = 7.6 Hz, 2H), 1.88-1.80 (m, 2H), 1.79-1.73 (m, 2H), 1.42-1.27 (m, 14H); ^{13}C NMR (100 MHz, $CDCl_3$) δ 188.6, 157.4, 153.3, 150.1, 146.3, 137.1, 126.8, 124.1, 120.4, 39.1, 34.1, 32.8, 29.4, 29.3, 29.2, 29.1, 28.7, 28.1, 24.0; HRMS calcd for $C_{20}H_{28}BrN_2O_2$ $(M + H)^+$ 407.1334; found 407.1331.

*12-fluoro-1-(5-(pyridin-2-yl)oxazol-2-yl)dodecan-1-one (**27**).* A solution of 18-crown-6 (486 mg, 1.84 mmol) in anhydrous CH_3CN (5.5 mL) was heated at 85 °C for 10 min, then KF (110 mg, 1.88 mmol) was added into the hot solution. And the mixture was stirred at 85 °C for 20 min. After that, compound **26** (150 mg, 0.37 mmol) was added, and the vessel was sealed tightly. The mixture was stirred at 95 °C for 42 h, then quenched with saturated aqueous NH_4Cl (10 mL) and extracted with Et_2O (3 x 10 mL). The combined organic portion was washed with brine (2 × 10 mL), dried over Na_2SO_4, filtered, and concentrated in vacuo. The residue was purified by flash chromatography on silica gel (hexanes to ethyl acetate gradient column) to yield the crude compound, which was recrystallized using 10% CH_2Cl_2/pentane to yield pure compound **27** as a white solid (38 mg, 30%). R_f = 0.25 (Hexanes/EtOAc = 10/1); ^{1}H NMR (400 MHz, $CDCl_3$) δ 8.67-8.65 (m, 1H), 7.88-7.85 (m, 2H), 7.80 (td, J = 7.6, 2.0 Hz, 1H), 7.33-7.29 (m, 1H), 4.43 (dt, J = 47.2, 6.4 Hz, 2H), 3.11 (t, J = 7.2 Hz, 2H), 1.79-1.70 (m, 2H), 1.69-1.61 (m, 2H), 1.40-1.24 (m, 14H); ^{13}C NMR (100 MHz, $CDCl_3$) δ 188.6, 157.4, 153.3, 150.1, 146.3, 137.1, 126.8, 124.1, 120.4, 84.2 (d, J_{C-F} = 163.1 Hz), 39.1, 30.5, 30.3, 29.4, 29.3, 29.2, 29.1, 25.1, 25.0, 24.0; ^{19}F NMR

(376 MHz, $CDCl_3$) δ -217.9; HRMS calcd for $C_{20}H_{28}FN_2O_2$ $(M + H)^+$ 347.2135; found 347.2129.

Radiolabeling of [^{11}C]MPPO. Carbon-11 CO_2 was produced by $^{14}N(p, \alpha)^{11}C$ nuclear reaction using a CYPRIS HM18 cyclotron (Sumitomo Heavy Industry, Tokyo, Japan). [^{11}C]Methyl iodide ([^{11}C]CH_3I) was synthesized from cyclotron-produced [^{11}C]CO_2. Briefly, [^{11}C]CO_2 was bubbled into a solution of $LiAlH_4$ (0.4 M in THF, 300 µL). After evaporation, the remaining reaction mixture was treated with hydroiodic acid (57% aqueous solution, 300 µL). The resulting [^{11}C]CH_3I was transferred under helium gas with heating into a pre-cooled (-15 to -20 °C) reaction vessel containing precursor **23** (1 mg), NaOH (6 µL, 0.5 M) and anhydrous DMF (300 µL). After the radioactivity reached a plateau during transfer, the reaction vessel was warmed to 80 °C and maintained for 5 min. CH_3CN / 0.05M NH_4OAc (v/v, 2/8, 1 mL) was added to the reaction mixture, which was then injected to a semi-preparative HPLC system. HPLC purification was completed on a Capcell Pak C18 column (10 mm ID × 250 mm; Shiseido, Tokyo) using a mobile phase of CH_3CN / 0.05M NH_4OAc (v/v, 2/8) at a flowrate of 5.0 mL/min. The retention time for [^{11}C]MPPO was 9.5 min, whereas that for unreacted **23** was 5.1 min. The radioactive fraction corresponding to the desired product was collected in a sterile flask, evaporated to dryness *in vacuo*, re-dissolved in sterile normal saline (3 mL), and passed through a 0.22 µm Millipore filter. The synthesis time was *ca.* 27 min from end-of-bombardment. Radiochemical and chemical purity were measured by analytical HPLC (Capcell Pak C18, 4.6 mm ID × 250 mm, UV at 254 nm; CH_3CN / 0.05M NH_4OAc (v/v, 2/8) ; retention time 8.5 min, 1.0 mL/min). The identity of [^{11}C]MPPO was confirmed by the co-injection with unlabeled MPPO. The specific activity of [^{11}C]MPPO was calculated based on a mass calibration curve at 254 nm. Radiochemical yield was 41% decay-corrected based on [^{11}C]CO_2 with >99% radiochemical purity and 2.2 Ci/µmol specific activity.

Measurement of Lipophilicity. The Log*D* value was measured by mixing [^{11}C]MPPO (radiochemical purity: 100%; approximately 150,000 cpm) with *n*-octanol (3.0 g) and a sodium phosphate-buffered saline (PBS, 3.0 g; 0.1 M, pH 7.40) in a test tube. The tube was vortexed for 3 min at room temperature, followed by centrifugation at 3500 rpm for 5 min. An aliquot of 0.65 mL PBS and 0.65 mL *n*-octanol was removed, weighted, and its radioactivity was counted using a 1480 Wizard autogamma counter (PerkinElmer, Waltham, MA), respectively. Each sample from the remaining organic layer were removed and re-partitioned until consistent Log*D* value was obtained. The Log*D* value was calculated by comparing the ratio of cpm/g of *n*-octanol to that of PBS and expressed as LogD = Log [cpm/g (*n*-octanol)/cpm/g (PBS)]. All assays were performed in triplicate.

Animal experiments. DdY mice (male; 7 weeks old; 34–36 g), and Sprague-Dawley (male; 7 weeks old; 210–230 g) rats were purchased from Japan SLC (Shizuoka, Japan). Wild-type (male; 17–18 weeks old; 30–32 g) and Pgp/Bcrp knockout (Abcb1a/1b$^{-/-}$Abcg2$^{-/-}$; male; 17–18 weeks old; 31–33 g) FAB mice were purchased from Taconic Farm (Hudson, NY). These animals were housed under a 12 h dark-light cycle and were allowed free access to food pellets and water. The animal experiments were approved by the Animal Ethics Committee of Massachusetts General Hospital and/or the National Institute of Radiological Sciences.

Biodistribution in mice. A saline solution of [^{11}C]MPPO (2 MBq, 0.03 nmol/200 µL) was injected into ddy mice via tail vein. Three mice were sacrificed at 1, 5, 15, 30, and 60 min after injection. Whole brain, heart, lung, liver, spleen, kidneys, small intestine (including contents), muscle, testes, and blood samples were quickly removed and weighed. The radioactivity present in these tissues was measured using a gamma counter, and all radioactivity measurements were decay corrected. The uptake of each organ is expressed as a percentage of the injected dose per gram of wet tissue (% ID/g).

Small-animal PET study in rats. PET scans were performed using a small-animal Inveon PET scanner (Siemens Medical Solutions USA, Knoxville, TN), which provides 159 transaxial slices 0.796 mm (center to center) apart, a 10 cm transaxial field of view (FOV), and a 12.7 cm axial FOV. Prior to imaging studies, Sprague-Dawley rats were anesthetized with 5% (v/v) isoflurane and maintained by 1-2% (v/v) isoflurane. To inject [^{11}C]MPPO, a 24-gauge needle with catheter (Terumo Medical Products, Tokyo) was placed into the rat tail vein. Emission scans were acquired for 90 min in three-dimensional list mode with an energy window of 350-750 keV, immediately after intravenous injection of [^{11}C]MPPO (40-51 MBq, 0.7-1 nmol/200 µL). For the pretreatment studies, unlabeled URB597 (3.0 mg/kg) dissolved in 300 µL saline containing 10% ethanol and 5% Tween® 80) were injected at 30 min before the injection of [^{11}C]MPPO. Three rats were used for each experiment.

PET dynamic images were reconstructed with filtered back-projection using a Hanning's filter, a Nyquist cutoff of 0.5 cycle/pixel. The PET images were reconstructed using ASIPro VM software (Analysis Tools and System Setup/Diagnostics Tool, Siemens Medical Solutions). All list-mode acquisition data were sorted into three-dimensional sinograms, which were then Fourier rebinned into two-dimensional sinograms (1 min × 4 scans, 2 min × 8 scans, 5 min × 8 scans). Regions of interest were placed on the whole brain, cerebral cortex and cerebellum using ASIPro VM. Regional brain uptake of radioactivity was decay-corrected to the injection time and was expressed as the standardized uptake value (SUV), which was normalized to the injected radioactivity and body weight. SUV = (radioactivity per mL tissue/injected radioactivity) × g body weight.

Small-animal PET study in mice. A wide-type or Pgp/Bcrp knockout FAB mouse was secured in a custom-designed chamber, placed in the Inveon PET scanner, and prepared as described above. A 29-gauge needle with 12–15 cm of polyethylene 10 tube prepared in house was placed into the tail vein of mouse to inject [^{11}C]MPPO (18 MBq, 0.12 nmol/100 µL). A dynamic emission scan in 3D list mode was performed for 60 min (1 min × 4 scans, 2 min × 8 scans, 5 min × 8 scans). Three mice were used for

each experiment, respectively. The PET data were treated as above.

Metabolite assay for rat plasma and brain homogenate. Following the intravenous injection of [^{11}C]MPPO (82 MBq, 1.1 nmol/200 μL), Sprague-Dawley rats (n = 3) were sacrificed by cervical dislocation at 15 min. Blood and whole brain samples were quickly removed and the blood samples were centrifuged at 15,000 g for 2 min at 4 °C to separate the plasma. The supernatant (0.5 mL) was then collected in a test tube containing CH_3CN (0.5 mL) and the resulting mixture was vortexed for 15 s and centrifuged at 15,000 g for 2 min for deproteinization. The rat brain was homogenized in an ice-cooled CH_3CN/H_2O (1/1, 1 mL) solution. The homogenate was centrifuged at 150,000 rpm for 2 min at 4 °C and the supernatant was collected. The recovery of radioactivity into the supernatant was > 90% based on the total radioactivity in the brain homogenate.

An aliquot of the supernatant (100–500 μL) obtained from the plasma or brain homogenate was injected into the radio-HPLC system, and analyzed under the same analytical conditions described above, except the flow rate of 2 mL/min. The percentage of [^{11}C]MPPO (retention time: 4.6 min) to total radioactivity (corrected for decay) on the HPLC charts was calculated as (peak area for [^{11}C]MPPO/total peak area) × 100.

■ ASSOCIATED CONTENT

Supporting Information

Characterization of all new compounds. This material is available free of charge via the Internet at http://pubs.acs.org.

■ AUTHOR INFORMATION

Corresponding Author

* Tel: +81 433 823 709. Fax: +81-43-206-3261. E-mail: zhang@nirs.go.jp.
* Tel: +1 617 726 6106. Fax: +1 617 726 6165. E-mail: liang.steven@mgh.harvard.edu.

Author Contributions

The manuscript was written through contributions of all authors. All authors have given approval to the final version of the manuscript.

Notes

The authors declare no competing financial interest.

■ ACKNOWLEDGMENTS

We would like to thank the staff at the radiochemistry program, Nuclear Medicine and Molecular Imaging, Massachusetts General Hospital, MA, USA and National Institute of Radiological Sciences, Chiba, Japan for their support with cyclotron operation, radioisotope production, radiosynthesis and animal experiments. S.H.L is a recipient of an NIH career development award (NIH/NIDA K01DA038000).

■ ABBREVIATIONS

PET, positron emission tomography; AEA, anandamide; 2-AG, 2-arachidonoylglycerl; FAAH, fatty acid amide hydrolase; MAGL, monoacylglycerol lipase; SUV, standardized uptake value, TAC, time-activity curve; %ID/g, percentage of injected dose per gram of wet tissue; SUV, standard uptake value; KO, knockout; PgP, P-glucoprotein; Bcrp, breast cancer resistance protein; 18-crown-6, 1,4,7,10,13,16-hexaoxacyclooctadecane; PPTS, Pyridinium *p*-toluenesulfonate; LiHMDS, Lithium bis(trimethylsilyl)amide; THF, tetrahydrofuran; DMF, dimethylformamide; DMSO, Dimethyl sulfoxide.

■ REFERENCES

(1) Ahn, K., McKinney, M.K. and Cravatt, B.F. (2008) Enzymatic Pathways That Regulate Endocannabinoid Signaling in the Nervous System. *Chem. Rev. 108*, 1687-1707.

(2) Devane, W.A., Hanus, L., Breuer, A., Pertwee, R.G., Stevenson, L.A., Griffin, G., Gibson, D., Mandelbaum, A., Etinger, A. and Mechoulam, R. (1992) Isolation and structure of a brain constituent that binds to the cannabinoid receptor. *Science 258*, 1946-1949.

(3) Mechoulam, R., Ben-Shabat, S., Hanus, L., Ligumsky, M., Kaminski, N.E., Schatz, A.R., Gopher, A., Almog, S., Martin, B.R., Compton, D.R. and et al. (1995) Identification of an endogenous 2-monoglyceride, present in canine gut, that binds to cannabinoid receptors. *Biochem. Pharmacol. 50*, 83-90.

(4) Sugiura, T., Kondo, S., Sukagawa, A., Nakane, S., Shinoda, A., Itoh, K., Yamashita, A. and Waku, K. (1995) 2-Arachidonoylglycerol: a possible endogenous cannabinoid receptor ligand in brain. *Biochem. Biophys. Res. Commun. 215*, 89-97.

(5) Ahn, K., Johnson, D.S. and Cravatt, B.F. (2009) Fatty acid amide hydrolase as a potential therapeutic target for the treatment of pain and CNS disorders. *Expert Opinion on Drug Discovery 4*, 763-784.

(6) Minkkila, A., Saario, S. and Nevalainen, T. (2010) Discovery and development of endocannabinoid-hydrolyzing enzyme inhibitors. *Curr. Top. Med. Chem. 10*, 828-858.

(7) Khanna, I.K. and Alexander, C.W. (2011) Fatty acid amide hydrolase inhibitors--progress and potential. *CNS Neurol. Disord. Drug Targets 10*, 545-558.

(8) Otrubova, K., Ezzili, C. and Boger, D.L. (2011) The Discovery and Development of Inhibitors of Fatty Acid Amide Hydrolase (FAAH). *Biorg. Med. Chem. Lett. 21*, 4674-4685.

(9) Blankman, J.L. and Cravatt, B.F. (2013) Chemical probes of endocannabinoid metabolism. *Pharmacol. Rev. 65*, 849-871.

(10) Gulyas, A.I., Cravatt, B.F., Bracey, M.H., Dinh, T.P., Piomelli, D., Boscia, F. and Freund, T.F. (2004) Segregation of two endocannabinoid-hydrolyzing enzymes into pre- and postsynaptic compartments in the rat hippocampus, cerebellum and amygdala. *Eur. J. Neurosci. 20*, 441-458.

(11) McKinney, M.K. and Cravatt, B.F. (2005) Structure and function of fatty acid amide hydrolase. *Annu. Rev. Biochem. 74*, 411-432.

(12) Bracey, M.H., Hanson, M.A., Masuda, K.R., Stevens, R.C. and Cravatt, B.F. (2002) Structural adaptations in a membrane enzyme that terminates endocannabinoid signaling. *Science 298*, 1793-1796.

(13) Lichtman, A.H., Shelton, C.C., Advani, T. and Cravatt, B.F. (2004) Mice lacking fatty acid amide hydrolase exhibit a cannabinoid receptor-mediated phenotypic hypoalgesia. *Pain 109*, 319-327.

(14) Gobbi, G., Bambico, F.R., Mangieri, R., Bortolato, M., Campolongo, P., Solinas, M., Cassano, T., Morgese, M.G., Debonnel, G., Duranti, A., Tontini, A., Tarzia, G., Mor, M., Trezza, V., Goldberg, S.R., Cuomo, V. and Piomelli, D. (2005) Antidepressant-like activity and modulation of brain monoaminergic transmission by blockade of anandamide hydrolysis. *Proc. Natl. Acad. Sci. U. S. A. 102*, 18620-18625.

(15) Gaetani, S., Dipasquale, P., Romano, A., Righetti, L., Cassano, T., Piomelli, D. and Cuomo, V. (2009) The endocannabinoid system

as a target for novel anxiolytic and antidepressant drugs. *Int. Rev. Neurobiol. 85*, 57-72.
(16) Kathuria, S., Gaetani, S., Fegley, D., Valino, F., Duranti, A., Tontini, A., Mor, M., Tarzia, G., La Rana, G., Calignano, A., Giustino, A., Tattoli, M., Palmery, M., Cuomo, V. and Piomelli, D. (2003) Modulation of anxiety through blockade of anandamide hydrolysis. *Nat. Med. 9*, 76-81.
(17) Piomelli, D. (2003) The molecular logic of endocannabinoid signalling. *Nat. Rev. Neurosci. 4*, 873-884.
(18) Johnson, D.S., Stiff, C., Lazerwith, S.E., Kesten, S.R., Fay, L.K., Morris, M., Beidler, D., Liimatta, M.B., Smith, S.E., Dudley, D.T., Sadagopan, N., Bhattachar, S.N., Kesten, S.J., Nomanbhoy, T.K., Cravatt, B.F. and Ahn, K. (2011) Discovery of PF-04457845: A Highly Potent, Orally Bioavailable, and Selective Urea FAAH Inhibitor. *ACS Med Chem Lett 2*, 91-96.
(19) Ahn, K., Smith, S.E., Liimatta, M.B., Beidler, D., Sadagopan, N., Dudley, D.T., Young, T., Wren, P., Zhang, Y., Swaney, S., Van Becelaere, K., Blankman, J.L., Nomura, D.K., Bhattachar, S.N., Stiff, C., Nomanbhoy, T.K., Weerapana, E., Johnson, D.S. and Cravatt, B.F. (2011) Mechanistic and pharmacological characterization of PF-04457845: a highly potent and selective fatty acid amide hydrolase inhibitor that reduces inflammatory and noninflammatory pain. *J. Pharmacol. Exp. Ther. 338*, 114-124.
(20) Li, G.L., Winter, H., Arends, R., Jay, G.W., Le, V., Young, T. and Huggins, J.P. (2012) Assessment of the pharmacology and tolerability of PF-04457845, an irreversible inhibitor of fatty acid amide hydrolase-1, in healthy subjects. *Br. J. Clin. Pharmacol. 73*, 706-716.
(21) Huggins, J.P., Smart, T.S., Langman, S., Taylor, L. and Young, T. (2012) An efficient randomised, placebo-controlled clinical trial with the irreversible fatty acid amide hydrolase-1 inhibitor PF-04457845, which modulates endocannabinoids but fails to induce effective analgesia in patients with pain due to osteoarthritis of the knee. *Pain 153*, 1837-1846.
(22) Postnov, A., Schmidt, M., Penson, J., Van Hecken, A., Zannikos, P., Pemberton, D., Palmer, J., de Hoon, J., Bormans, G. and Van Laere, K. (2015) Kinetic modeling of Fatty Acid Amide Hydrolase (FAAH) enzyme occupancy after JNJ-42165279 inhibition based on [^{11}C]MK-3168 PET imaging of human brain. *Journal of Nuclear Medicine Meeting Abstracts 56*, 362.
(23) ClinicalTrials. Identifier, NCT01634529.
(24) Wyffels, L., Muccioli, G.G., De Bruyne, S., Moerman, L., Sambre, J., Lambert, D.M. and De Vos, F. (2009) Synthesis, in vitro and in vivo evaluation, and radiolabeling of aryl anandamide analogues as candidate radioligands for in vivo imaging of fatty acid amide hydrolase in the brain. *J. Med. Chem. 52*, 4613-4622.
(25) Wyffels, L., Muccioli, G.G., Kapanda, C.N., Labar, G., De Bruyne, S., De Vos, F. and Lambert, D.M. (2010) PET imaging of fatty acid amide hydrolase in the brain: synthesis and biological evaluation of an ^{11}C-labelled URB597 analogue. *Nucl. Med. Biol. 37*, 665-675.
(26) Wilson, A.A., Garcia, A., Parkes, J., Houle, S., Tong, J. and Vasdev, N. (2011) [^{11}C]CURB: Evaluation of a novel radiotracer for imaging fatty acid amide hydrolase by positron emission tomography. *Nucl. Med. Biol. 38*, 247-253.
(27) Wilson, A.A., Hicks, J.W., Sadovski, O., Parkes, J., Tong, J., Houle, S., Fowler, C.J. and Vasdev, N. (2013) Radiosynthesis and Evaluation of [^{11}C-Carbonyl]-Labeled Carbamates as Fatty Acid Amide Hydrolase Radiotracers for Positron Emission Tomography. *J. Med. Chem. 56*, 201-209.
(28) Sadovski, O., Hicks, J.W., Parkes, J., Raymond, R., Nobrega, J., Houle, S., Cipriano, M., Fowler, C.J., Vasdev, N. and Wilson, A.A. (2013) Development and characterization of a promising fluorine-18 labelled radiopharmaceutical for in vivo imaging of fatty acid amide hydrolase. *Bioorg. Med. Chem. 21*, 4351-4357.
(29) Rotstein, B.H., Wey, H.Y., Shoup, T.M., Wilson, A.A., Liang, S.H., Hooker, J.M. and Vasdev, N. (2014) PET imaging of fatty acid amide hydrolase with [^{18}F]DOPP in nonhuman primates. *Mol. Pharm. 11*, 3832-3838.
(30) Hicks, J.W., Parkes, J., Sadovski, O., Tong, J., Houle, S., Vasdev, N. and Wilson, A.A. (2013) Synthesis and preclinical evaluation of [^{11}C-carbonyl]PF-04457845 for neuroimaging of fatty acid amide hydrolase. *Nucl. Med. Biol. 40*, 740-746.
(31) Liu, P., Hamill, T.G., Chioda, M., Chobanian, H., Fung, S., Guo, Y., Chang, L., Bakshi, R., Hong, Q., Dellureficio, J., Lin, L.S., Abbadie, C., Alexander, J., Jin, H., Mandala, S., Shiao, L.L., Li, W., Sanabria, S., Williams, D., Zeng, Z., Hajdu, R., Jochnowitz, N., Rosenbach, M., Karanam, B., Madeira, M., Salituro, G., Powell, J., Xu, L., Terebetski, J.L., Leone, J.F., Miller, P., Cook, J., Holahan, M., Joshi, A., O'Malley, S., Purcell, M., Posavec, D., Chen, T.B., Riffel, K., Williams, M., Hargreaves, R., Sullivan, K.A., Nargund, R.P. and DeVita, R.J. (2013) Discovery of MK-3168: A PET Tracer for Imaging Brain Fatty Acid Amide Hydrolase. *ACS Med. Chem. Lett. 4*, 509-513.
(32) Skaddan, M.B., Zhang, L., Johnson, D.S., Zhu, A., Zasadny, K.R., Coelho, R.V., Kuszpit, K., Currier, G., Fan, K.H., Beck, E.M., Chen, L., Drozda, S.E., Balan, G., Niphakis, M., Cravatt, B.F., Ahn, K., Bocan, T. and Villalobos, A. (2012) The synthesis and in vivo evaluation of [^{18}F]PF-9811: a novel PET ligand for imaging brain fatty acid amide hydrolase (FAAH). *Nucl. Med. Biol. 39*, 1058-1067.
(33) Kumata, K., Yui, J., Hatori, A., Maeda, J., Xie, L., Ogawa, M., Yamasaki, T., Nagai, Y., Shimoda, Y., Fujinaga, M., Kawamura, K. and Zhang, M.R. (2015) Development of [^{11}C]MFTC for PET imaging of fatty acid amide hydrolase in rat and monkey brains. *ACS Chem. Neurosci. 6*, 339-346.
(34) Rusjan, P.M., Wilson, A.A., Mizrahi, R., Boileau, I., Chavez, S.E., Lobaugh, N.J., Kish, S.J., Houle, S. and Tong, J. (2013) Mapping human brain fatty acid amide hydrolase activity with PET. *J. Cereb. Blood Flow Metab. 33*, 407-414.
(35) Boileau, I., Bloomfield, P.M., Rusjan, P., Mizrahi, R., Mufti, A., Vitcu, I., Kish, S.J., Houle, S., Wilson, A.A. and Tong, J. (2014) Whole-body radiation dosimetry of ^{11}C-carbonyl-URB694: a PET tracer for fatty acid amide hydrolase. *J. Nucl. Med. 55*, 1993-1997.
(36) Joshi, A., Li, W., Sanabria, S., Holahan, M., Purcell, M., Declercq, R., Depre, M., Bormans, G., Van Laere, K. and Hamill, T. (2012) Translational studies with [^{11}C]MK-3168, a PET tracer for fatty acid amide hydrolase (FAAH). *J Nucl. Med. Meeting Abstracts 53*, 397.
(37) Fowler, J.S., MacGregor, R.R., Wolf, A.P., Arnett, C.D., Dewey, S.L., Schlyer, D., Christman, D., Logan, J., Smith, M., Sachs, H. and et al. (1987) Mapping human brain monoamine oxidase A and B with 11C-labeled suicide inactivators and PET. *Science 235*, 481-485.
(38) Cumming, P. and Vasdev, N. The Assay of Enzyme Activity by Positron Emission Tomography. in *Molecular Imaging in the Clinical Neurosciences*, Vol. 71 (ed. Gründer, G.) 111-135 (Humana Press, 2012).
(39) Innis, R.B., Cunningham, V.J., Delforge, J., Fujita, M., Gjedde, A., Gunn, R.N., Holden, J., Houle, S., Huang, S.-C., Ichise, M., Iida, H., Ito, H., Kimura, Y., Koeppe, R.A., Knudsen, G.M., Knuuti, J., Lammertsma, A.A., Laruelle, M., Logan, J., Maguire, R.P., Mintun, M.A., Morris, E.D., Parsey, R., Price, J.C., Slifstein, M., Sossi, V., Suhara, T., Votaw, J.R., Wong, D.F. and Carson, R.E. (2007) Consensus nomenclature for in vivo imaging of reversibly binding radioligands. *J. Cereb. Blood Flow Metab. 27*, 1533-1539.
(40) Pike, V.W. (2009) PET Radiotracers: crossing the blood-brain barrier and surviving metabolism. *Trends Pharmacol. Sci. 30*, 431-440.
(41) Mileni, M., Garfunkle, J., DeMartino, J.K., Cravatt, B.F., Boger, D.L. and Stevens, R.C. (2009) Binding and inactivation mechanism of a humanized fatty acid amide hydrolase by alpha-ketoheterocycle inhibitors revealed from cocrystal structures. *J. Am. Chem. Soc. 131*, 10497-10506.
(42) Otrubova, K. and Boger, D.L. (2012) alpha-Ketoheterocycle-based Inhibitors of Fatty Acid Amide Hydrolase (FAAH). *ACS Chem. Neurosci. 3*, 340-348.
(43) Hardouin, C., Kelso, M.J., Romero, F.A., Rayl, T.J., Leung, D., Hwang, I., Cravatt, B.F. and Boger, D.L. (2007) Structure-activity relationships of alpha-ketooxazole inhibitors of fatty acid amide hydrolase. *J. Med. Chem. 50*, 3359-3368.
(44) Georgiades, S.N. and Rizeq, N. (2015) Synthesis of a 'Propeller-Like' Oligoheteroaryl with Alternating Pyridine and Oxazole Motifs. *Synlett 26*, 489-493.

(45) Boger, D.L., Miyauchi, H., Du, W., Hardouin, C., Fecik, R.A., Cheng, H., Hwang, I., Hedrick, M.P., Leung, D., Acevedo, O., Guimaraes, C.R., Jorgensen, W.L. and Cravatt, B.F. (2005) Discovery of a potent, selective, and efficacious class of reversible alpha-ketoheterocycle inhibitors of fatty acid amide hydrolase effective as analgesics. *J. Med. Chem. 48*, 1849-1856.

(46) Dishino, D.D., Welch, M.J., Kilbourn, M.R. and Raichle, M.E. (1983) Relationship between lipophilicity and brain extraction of C-11-labeled radiopharmaceuticals. *J. Nucl. Med. 24*, 1030-1038.

(47) Wilson, A.A., Jin, L., Garcia, A., DaSilva, J.N. and Houle, S. (2001) An admonition when measuring the lipophilicity of radiotracers using counting techniques. *Appl. Radiat. Isot. 54*, 203-208.

(48) Waterhouse, R.N. (2003) Determination of lipophilicity and its use as a predictor of blood-brain barrier penetration of molecular imaging agents. *Mol. Imaging Biol. 5*, 376-389.

(49) Zoghbi, S.S., Anderson, K.B., Jenko, K.J., Luckenbaugh, D.A., Innis, R.B. and Pike, V.W. (2012) On Quantitative Relationships Between Drug-Like Compound Lipophilicity and Plasma Free Fraction in Monkey and Human. *J. Pharm. Sci. 101*, 1028-1039.

(50) Watanabe, K., Ogi, H., Nakamura, S., Kayano, Y., Matsunaga, T., Yoshimura, H. and Yamamoto, I. (1998) Distribution and characterization of anandamide amidohydrolase in mouse brain and liver. *Life Sci. 62*, 1223-1229.

(51) Ueda, N., Puffenbarger, R.A., Yamamoto, S. and Deutsch, D.G. (2000) The fatty acid amide hydrolase (FAAH). *Chem. Phys. Lipids 108*, 107-121.

(52) Fowler, C.J., Jonsson, K.O. and Tiger, G. (2001) Fatty acid amide hydrolase: biochemistry, pharmacology, and therapeutic possibilities for an enzyme hydrolyzing anandamide, 2-arachidonoylglycerol, palmitoylethanolamide, and oleamide. *Biochem. Pharmacol. 62*, 517-526.

(53) Hillard, C.J., Wilkison, D.M., Edgemond, W.S. and Campbell, W.B. (1995) Characterization of the kinetics and distribution of N-arachidonylethanolamine (anandamide) hydrolysis by rat brain. *Biochim. Biophys. Acta 3*, 249-256.

(54) Thomas, E.A., Cravatt, B.F., Danielson, P.E., Gilula, N.B. and Sutcliffe, J.G. (1997) Fatty acid amide hydrolase, the degradative enzyme for anandamide and oleamide, has selective distribution in neurons within the rat central nervous system. *J. Neurosci. Res. 50*, 1047-1052.

(55) Tatsuta, T., Naito, M., Oh-hara, T., Sugawara, I. and Tsuruo, T. (1992) Functional involvement of P-glycoprotein in blood-brain barrier. *J. Biol. Chem. 267*, 20383-20391.

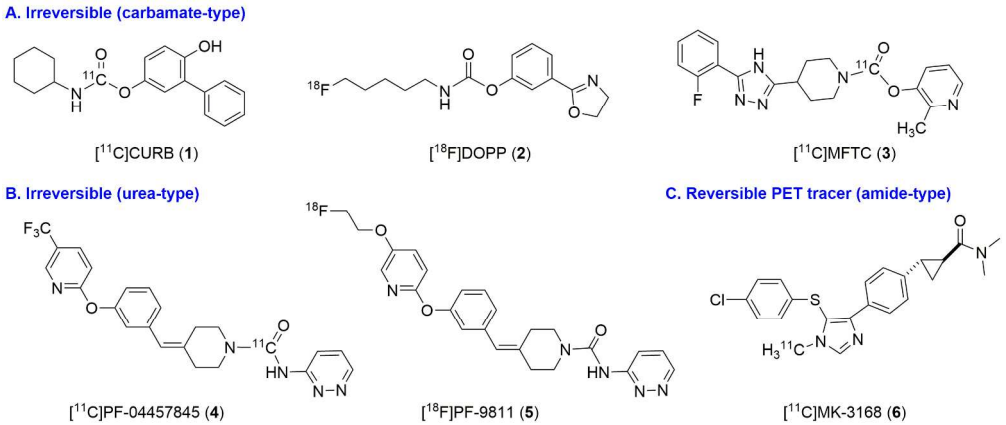

Figure 1.Representative PET radiotracers for imaging FAAH.
220x93mm (300 x 300 DPI)

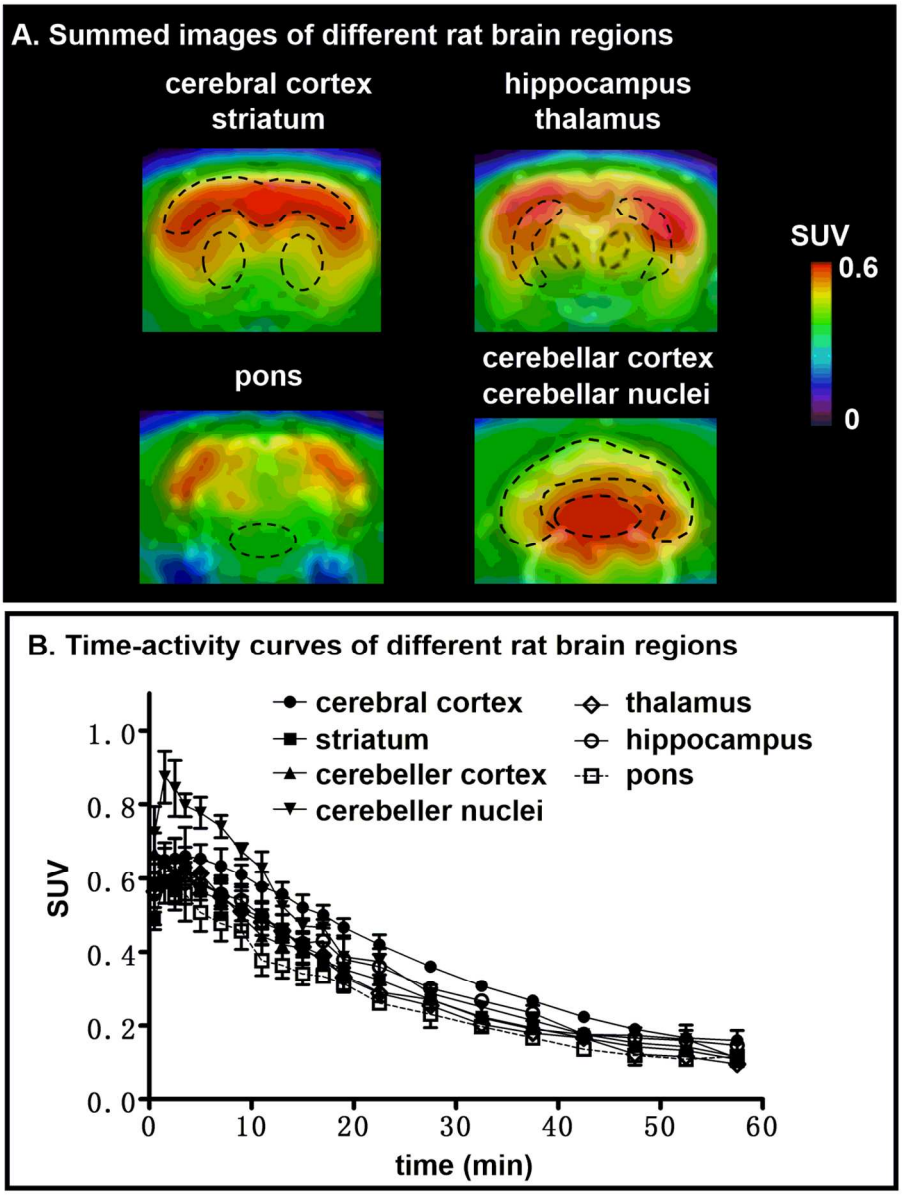

Figure 2.Representative coronal PET images (summed 0-30 min) and time-activity curves of [11C]MPPO in different rat brain regions (n = 3, mean ± SEM).
111x146mm (300 x 300 DPI)

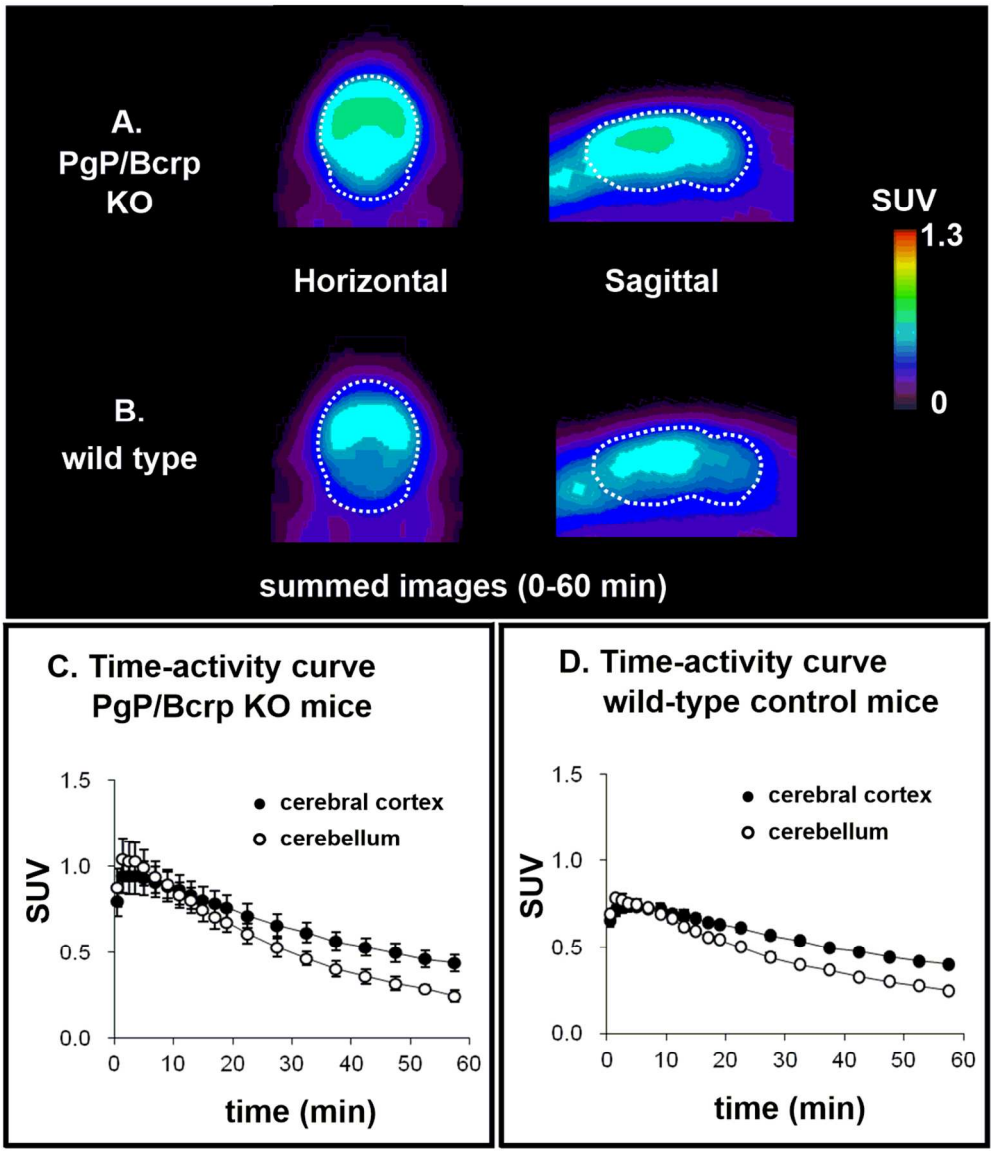

Figure 3.Representative PET images (0-30 min) and time-activity curves (baseline and blocking) of [11C]MPPO in rat brains. (n = 3; mean ± SEM).
111x128mm (300 x 300 DPI)

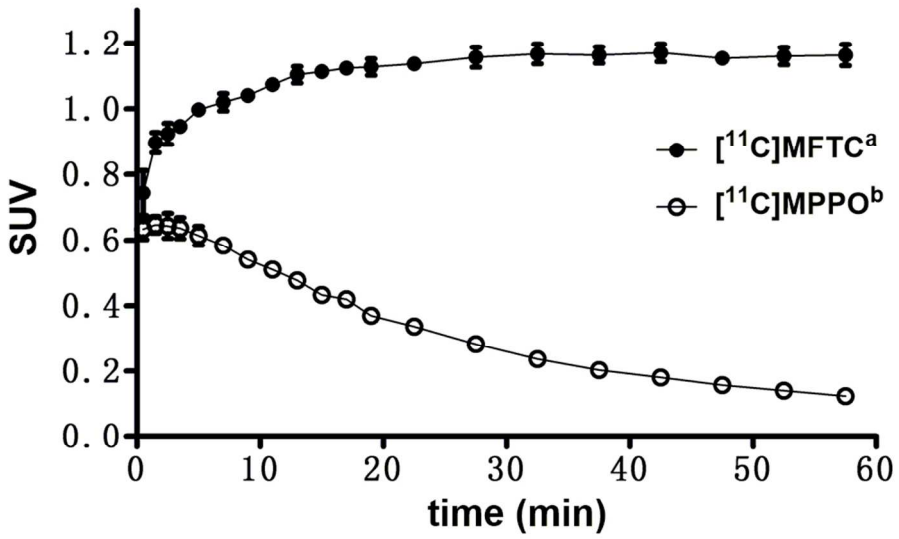

Figure 4.Reversible binding of [11C]MPPO in the brain. (n = 3; mean ± SD).
94x56mm (300 x 300 DPI)

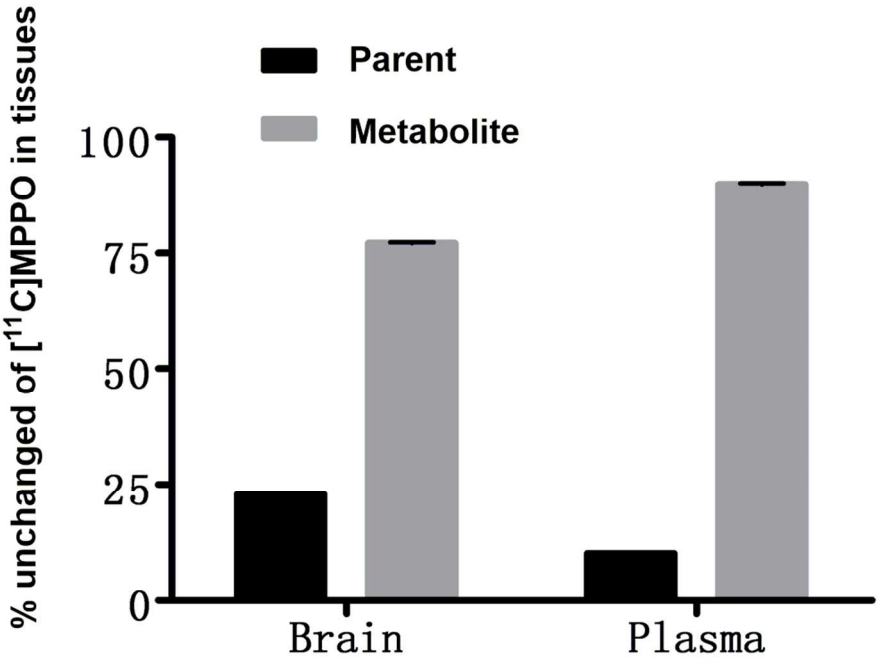

Figure 5. Radiometabolites of [11C]MPPO in rats. (n = 3; mean ± SD)
102x70mm (300 x 300 DPI)

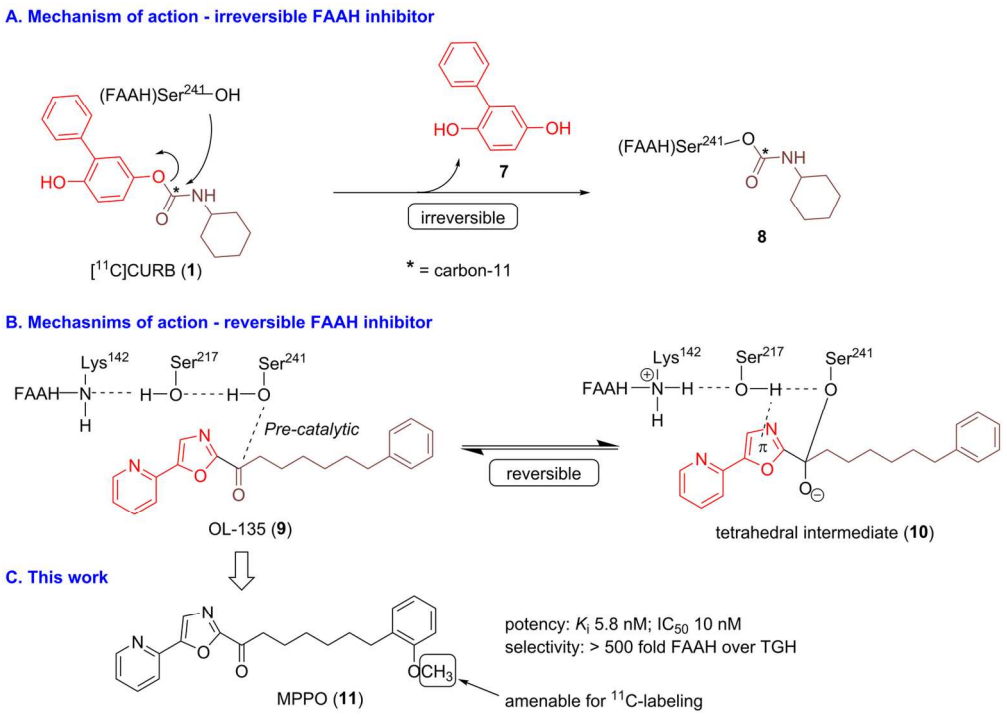

Scheme 1. Mechanism of action and this work.
145x103mm (300 x 300 DPI)

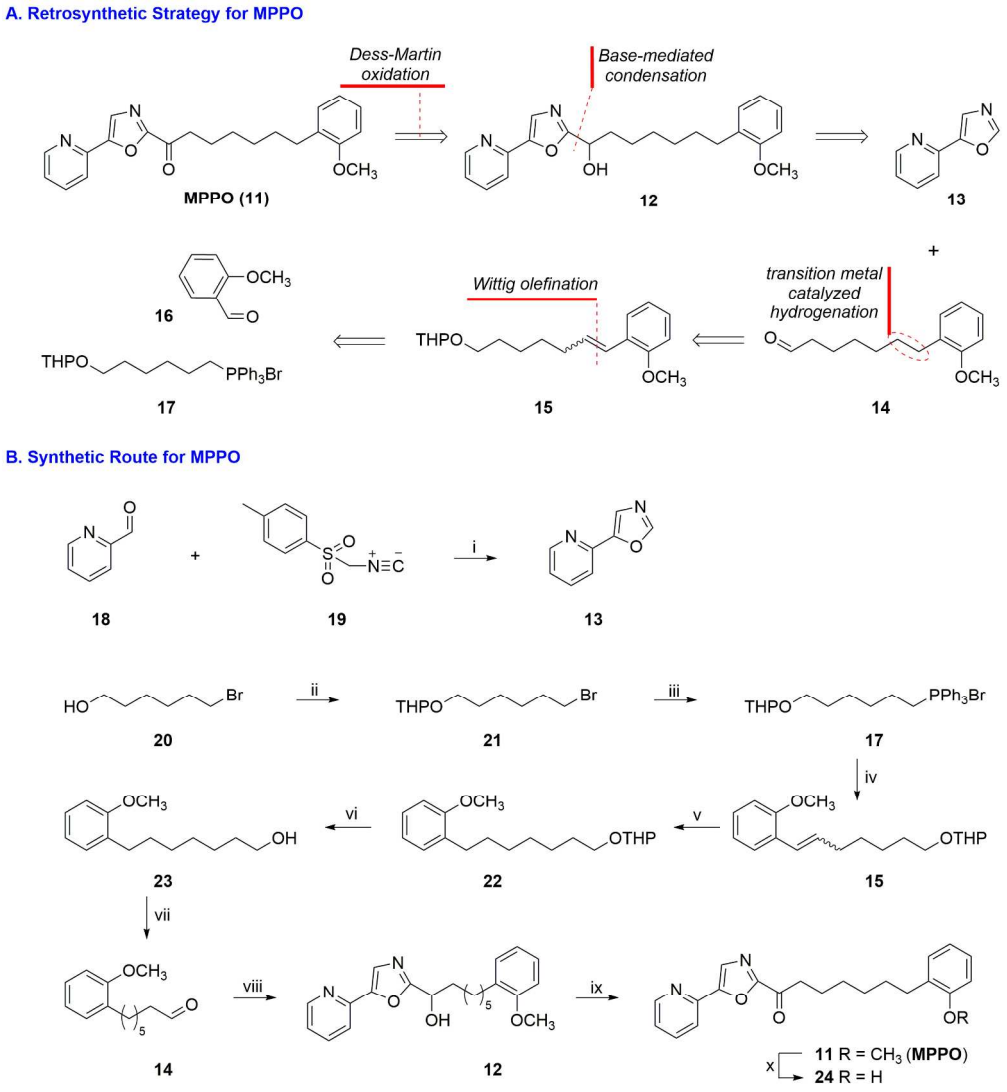

Scheme 2. (Retro)syntheses of standard and precursor molecules.
206x225mm (300 x 300 DPI)

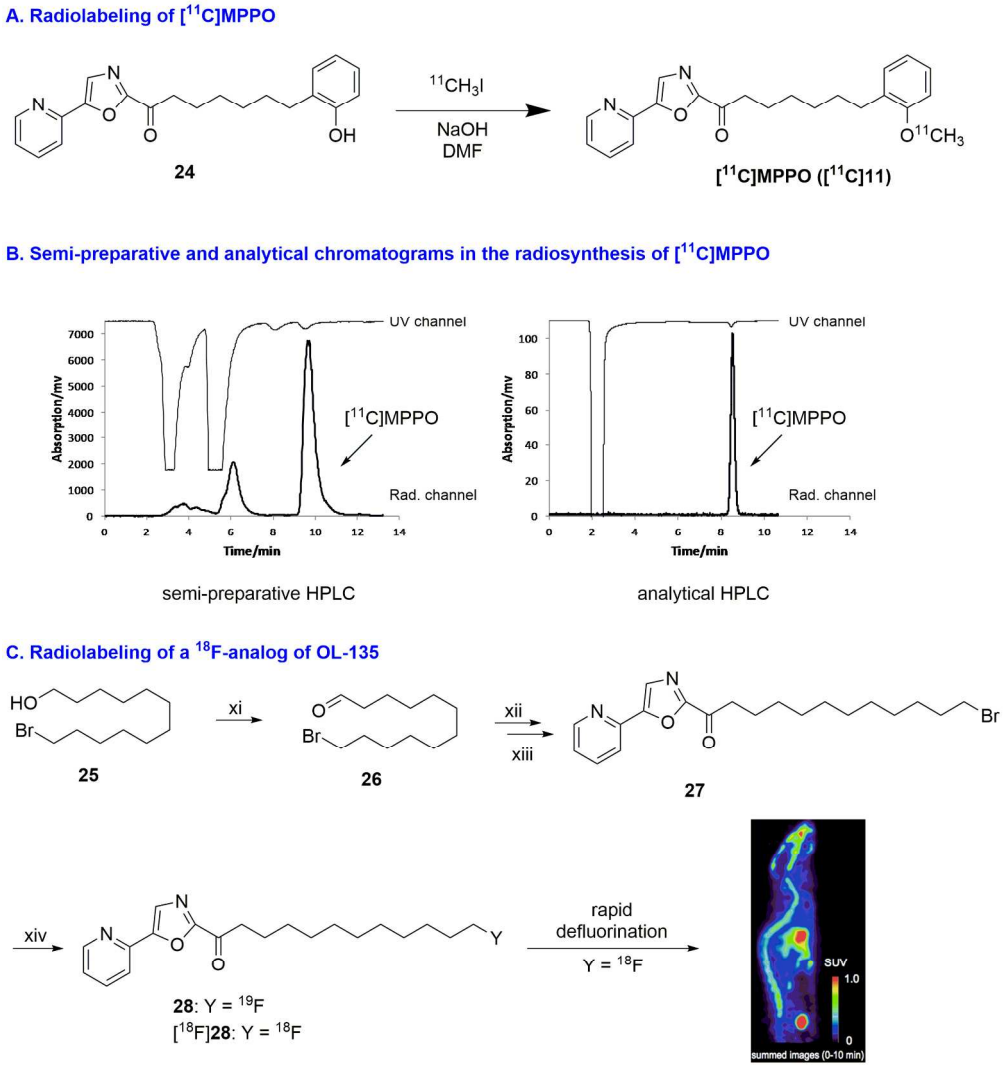

Scheme 3. Radiolabeling of FAAH radiotracers.
190x203mm (300 x 300 DPI)

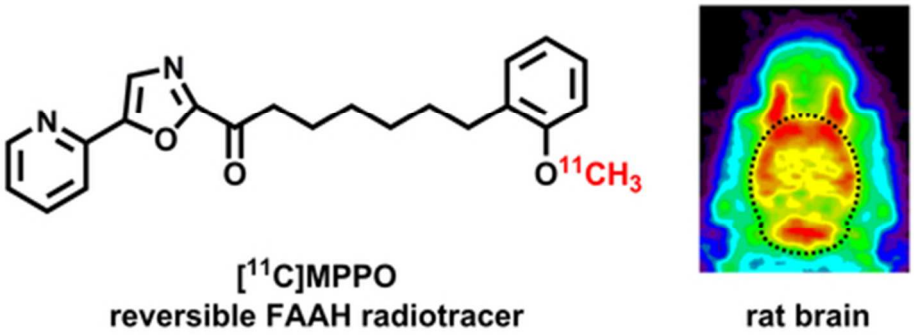

[^{11}C]MPPO
reversible FAAH radiotracer

rat brain

table of contents
38x14mm (300 x 300 DPI)